DESIGN AND PERFORMANCE EVALUATION OF A MEDIUM POWER PM-ASSISTED RELUCTANCE SYNCHRONOUS TRACTION MACHINE USING BONDED PM-SHEETS

S.E. Sibande, M.J. Kamper and R. Wang

Electrical Machines and Drives Laboratory, Department of Electrical and Electronic Engineering, University of Stellenbosch, Matieland, 7602, South Africa.

Abstract: This paper describes the optimum design of a permanent-magnet-assisted reluctance rotor of a 110 kW reluctance synchronous traction machine. Previous studies show that the performance of the pure reluctance synchronous machine drive deteriorates fast in the flux-weakening speed region. To address this problem, thin bonded permanent-magnet sheet material is used inside the flux barriers of the reluctance rotor to improve the performance of the drive, especially in the flux-weakening speed region. A design optimization algorithm is implemented to minimize the volume and hence the cost of the permanent-magnet material, subject to voltage and torque constraints. The calculated and measured results show clearly that the performance of the reluctance synchronous traction machine with a minimum amount of permanent-magnet material in the rotor compares favorably with the performance of the conventional induction machine drive at both rated and maximum speeds.

Key words: reluctance synchronous machine, finite element, optimisation, permanent magnet.

1. INTRODUCTION

The distinct features of induction machines (IMs) such as low cost, good performance over a fairly wide speed range and robust machine design have made them popular in variable-speed AC traction drives. Despite these advantages IMs suffer relatively high rotor losses, which affect the efficiency and starting tractive effort (short time current rating) of the drive; it also makes the cooling of the machine more difficult in principle. These inherent disadvantages of the IM drive have led engineers to seek alternate directions to find low cost AC traction drives without these disadvantages.

Comparative studies carried out on the performance of the reluctance synchronous machine (RSM) and IM in the low and medium power range show that the RSM has equal or higher torque density and higher efficiency [1 - 4]. The other features of RSMs which are considered advantageous over IMs may be summarized as follows: (i) it requires a simple vector control scheme due to the absence of rotor currents; (ii) it has insignificant rotor losses which implies that the cooling of the machine is much less of a problem and the rotor bearings run cooler; and (iii) the rotor manufacturing cost is relatively low. It is further known that inverter-fed IMs are de-rated due to additional harmonic copper losses in the rotor. These additional harmonic copper losses are not present in inverter-fed RSMs.

On the disadvantage side it has been shown that the RSM has a low power factor, which in turn calls for a high inverter rating to attain a wide constant-power speed range. A high inverter rating may increase the total cost of the RSM drive. Previous studies show that the performance of the RSM as compared to the IM deteriorates fast in the flux-weakening speed region [3 - 5].

To address this problem, permanent magnets (PMs) are usually placed inside the flux barriers of the reluctance rotor to improve the performance of the RSM drive, especially in the flux-weakening region. These drives are defined as PM-assisted RSM drives [6 - 10]. This paper describes the optimal design of a PM-assisted reluctance rotor of a 110 kW inverter-fed RSM for suburban train applications. The performance of this drive is compared with the performance of the equivalent IM traction drive.

2. PERFORMANCE OF IM AND RSM DRIVES

The performance comparison between the IM and RSM drives was done by using the same stator for both machines. Although using the same stator penalises the RSM's performance in general, it is important for the industry to know the performance difference between these drives when replacing only the rotor. A cross-section of the 110 kW, optimum designed RSM is shown in Fig. 1. The 6-pole stator with 54 slots has a three-phase double-layer chorded winding with an 8/9 pitch. In the stator yoke are cooling ducts for circulating air within the machine using an internal shaft mounted fan. The reluctance rotor, also shown in Fig. 2, consists of laminated steel only with internal air openings called flux barriers. This rotor has been optimally designed using an optimisation algorithm and finite element analysis [3]. The IM's rotor shown in Fig. 3 has 48 slots and a copper single-cage winding.

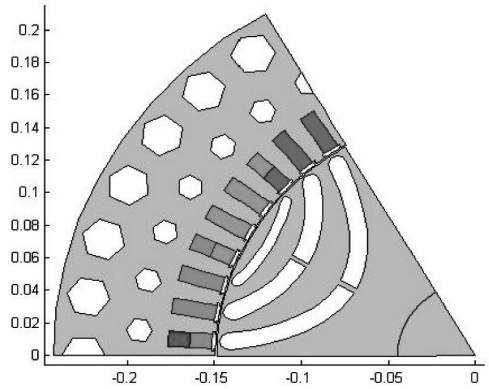

Figure 1: Cross-section of 110 kW RSM [3].

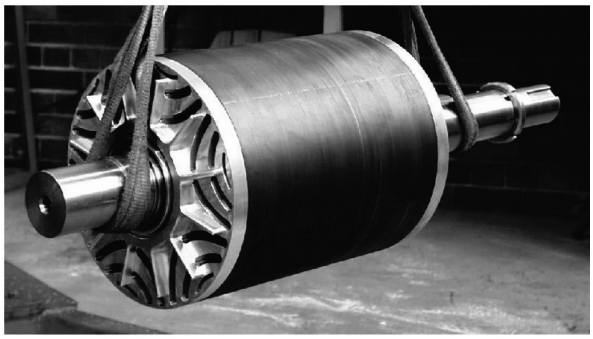

Figure 2: Assembled RSM's rotor [3].

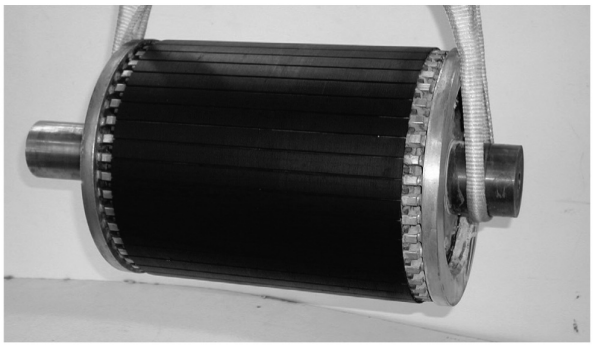

Figure 3: Assembled IM's rotor.

The torque versus speed performance of the RSM drive is compared in [4] with that of the IM drive with the supply voltage and stator current the same for both machines. The measured torque performances of both drives are shown in Fig. 4. It is clear that up to base speed, i.e. 1200 r/min [rated speed is 1500 r/min, but for testing the drives a lower base speed was selected], the torque of the RSM compares well with the torque of the IM for the same stator current. In the flux-weakening speed region, however, the generated torque of the RSM is poor compared to the torque of the IM; i.e. the torque of the RSM deteriorates fast under current and supply voltage constraints.

It should be noted that for the same total copper losses as that of the IM, the stator current of the RSM (using the same stator) could be raised by a factor

$$\left(\frac{P_{\text{total copper losses (IM)}}}{P_{\text{total copper losses (IM)}} - P_{\text{rotor copper losses (IM)}}} \right)^{1/2}. \qquad (1)$$

This will result in an increased torque of the RSM by almost the same factor (in [2] it is shown that the torque of the RSM is very much proportional to the stator current).

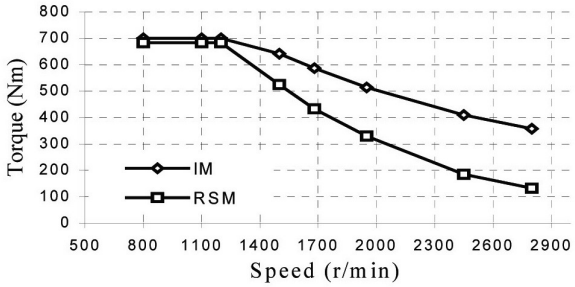

Figure 4: Rated torque versus speed performance of RSM and IM traction drives (drives were tested up to 88 kW only) [4].

3. RSM WITH PM-ASSISTED

In order to improve the performance of the RSM, especially in the flux weakening speed region, it has been proposed by some researchers that a small quantity of PM material may be incorporated into the reluctance rotor to reduce the q-axis magnetic flux and in this way increase the magnetic saliency of the machine [6 - 10]. These are well-designed reluctance machines with only a small amount of PM material to keep cost and no-load induced voltage low. Sometimes these machines are also called interior PM machines, but with interior PM machines [11] the focus in general is on PM machines with only a small amount of reluctance torque and power; the authors, therefore, distinguishes between these two machines. Figure 5 shows the reluctance rotor of the 110 kW RSM under study with thin 3 mm PM sheets inside the three flux barriers of the reluctance rotor.

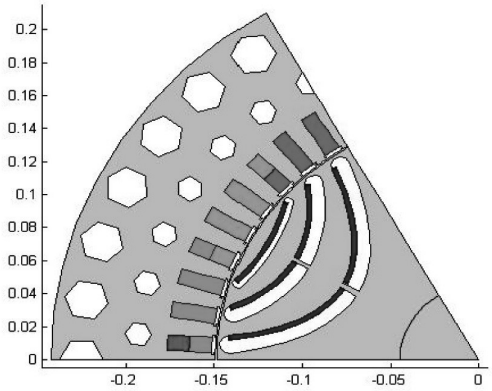

Figure 5: Cross section of 110 kW RSM with PM sheets incorporated in the reluctance rotor.

From classical texts on *dq*-axis theory the steady-state *dq* voltage equations of the PM-assisted RSM are given by

$$V_d = R_s I_d - \omega\lambda_q + \omega\lambda_{pm} \quad (2)$$

$$V_q = R_s I_q + \omega\lambda_d\,, \quad (3)$$

where I_d and I_q are the steady state *dq* currents, R_s is the stator phase resistance, λ_d and λ_q are the *dq* flux linkages, λ_{pm} is the flux linkage due to the PMs and ω is the electrical speed of the rotor. The flux linkages are defined as

$$\lambda_d = L_d I_d \quad (4)$$

$$\lambda_q = L_q I_q\,, \quad (5)$$

where L_d and L_q are the *dq*-axis inductances. From equations (2) and (3) the steady state *d*- and *q*-axis equivalent circuits of the PM-assisted RSM can be obtained, as shown in Fig. 6. In Fig. 7 the steady-state vector diagrams of both the RSM and PM-assisted RSM are shown. From eqns (2) and (3) and the equivalent circuits of Fig. 6 the developed torque of the machine can be derived and expressed as

$$T = \tfrac{3}{2}\,p\left(L_d - L_q\right)I_d I_q + \tfrac{3}{2}\,p\lambda_{pm} I_d \quad (6)$$

or else

$$T = \frac{3}{4}\,p\left(L_d + \frac{\lambda_{pm}}{I_q} - L_q\right)I_s^2 \sin(2\phi)\,, \quad (7)$$

where p is the number of pole pairs and φ is the current angle between the current space phasor and the *d*-axis of the rotor as shown in Fig 7. The first term in equation (6) expresses the reluctance torque component of the machine, while the second term expresses the torque due to permanent magnet excitation. Note that for the machine of Fig. 5, $L_d > L_q$, which implies that both I_d and I_q must be positive to generate a positive reluctance torque. The PM-term of equation (6) is zero in the case of a pure RSM.

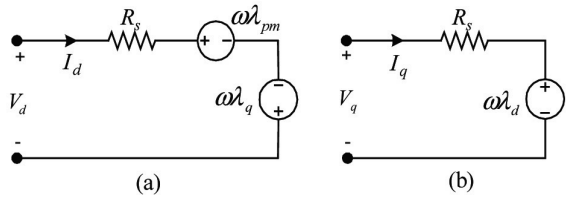

Figure 6: Steady state *d*-axis (a) and *q*-axis (b) equivalent circuits of PM-assisted RSM.

Finite element (fe) analysis is used to do some initial performance calculations on the machine of fig. 5 To study the effect of the added pm sheets. Thin 3 mm pm sheets with different magnet strengths are used in the analysis.

The fe calculated results of torque and voltage versus current angle [the current angle is defined in fig. 7] Of the pm-assisted rsm are shown in figs. 8 And 9 respectively. It is clear from fig. 8 That with the pm-material added, the torque of the rsm improves significantly, up to 23% if strong magnets are used. The optimum current angle also reduces from 57 to 53º if strong magnets are used. Fig. 9

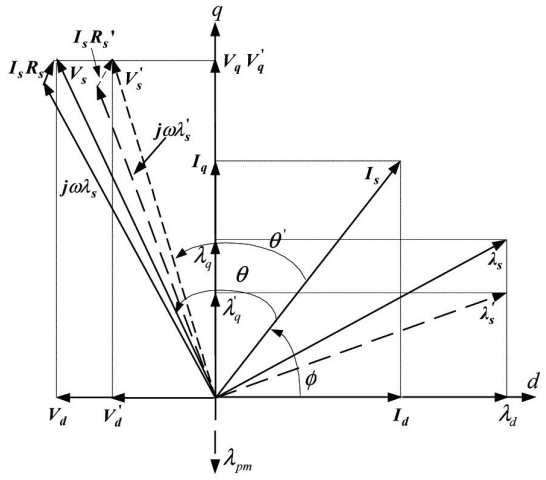

Figure 7: steady state vector diagrams of rsm (solid lines) and pm assisted rsm (dotted lines and accents for symbols).

Shows that the supply voltage of the machine is reduced by the pm-material, especially at high current angles, i.E. In the flux-weakening mode of the drive. This result is very important, as it will widen the high speed or constant power speed range of the drive.

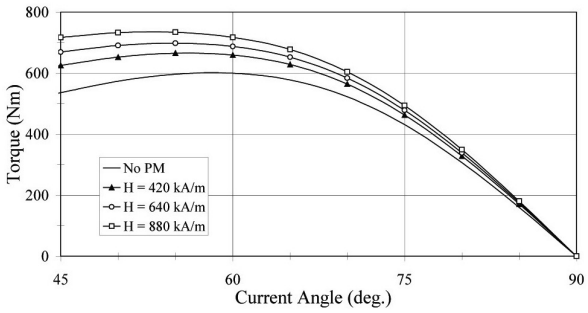

Figure 8: Torque versus current angle at 187 A *rms* with magnet strength a parameter.

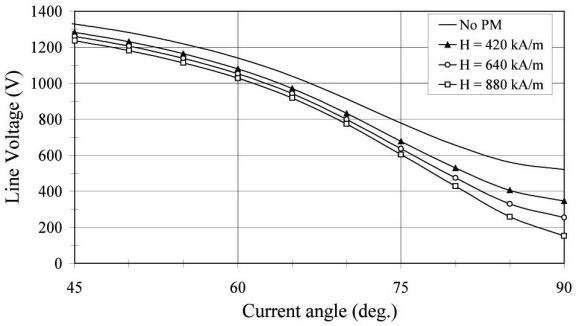

Figure 9: Line voltage versus current angle at 187 A *rms* and 3800 r/min with magnet strength a parameter.

4. DESIGN OPTIMISATION

To minimise the cost of the PM-assisted RSM it is important to minimise the amount of magnet material used in the RSM-rotor of Fig. 5, subject to torque and supply voltage constraints of the electrical drive. Hence, a constraint optimisation algorithm is necessary, but also FE analysis to calculate the torque and supply voltage of the machine accurately. A constrained optimisation problem can be solved as an unconstrained optimisation problem by adding penalty functions. This can be explained by the following equation:

$$Y = F(\boldsymbol{X},\boldsymbol{w}) = f(\boldsymbol{X}) + \sum_{i=1}^{n} w_i c_i(\boldsymbol{X}) \; . \qquad (8)$$

In this equation $\boldsymbol{X}$ is a variable matrix-vector, $f(\boldsymbol{X})$ is the objective function to be minimised, n is the number of penalty functions, $c_i(\boldsymbol{X})$ is the i-th penalty function and w_i is simply a weight that determines the extent by which the function is penalised. The optimisation algorithm, thus, finds the multi-dimensional vector $\boldsymbol{X}$ that minimises Y of equation (8).

In the case of minimising the volume of the magnets used in the rotor of Fig. 5, the thicknesses of the three magnet sheets, x_1, x_2 and x_3, are optimised. Hence, $\boldsymbol{X}$ in equation (8) represents the magnet thicknesses, i.e. $\boldsymbol{X} = [x_1\ x_2\ x_3]$. f($\boldsymbol{X}$) in equation (8) is the magnet volume to be minimised. Furthermore, as there are only two constraints, a torque constraint and a voltage constraint, there are only two penalty functions in this case. For both constraints a quadratic penalty function, $c_i(\boldsymbol{X}) = [u_o - u(\boldsymbol{X})]^2$, is used, where u represents in this case torque or voltage. Practically, equation (8) is implemented as follows, ensuring minimum required torque and maximum allowed supply voltage:

$$Y = F(\boldsymbol{X},\boldsymbol{w}) = Vol_{magnet} + w_1(V_o - V_s)^2 + w_2(T_o - T_{out})^2 \quad (9)$$

$$w_1 = \begin{cases} 0 & V_s \le V_o \\ 40 & V_s > V_o \end{cases} \qquad (10)$$

$$w_2 = \begin{cases} 0 & T_{out} \ge T_o \\ 40 & T_{out} < T_o \end{cases} \qquad (11)$$

In (9) Vol_{mag} is the magnet volume, V_s and T_{out} are respectively the FE calculated phase voltage and torque of the machine, and T_o and V_o are the required torque and maximum allowed voltage respectively at maximum speed (maximum speed in this case is 2800 r/min from Fig. 4).

The optimisation procedure used may be described by the flow diagram of Fig 10. In this procedure the Powell algorithm [12] is used. Furthermore, as shown in Fig. 10, the FE method is directly used in the optimisation procedure as described by [13]. With each iteration r the algorithm determines directions of search in a multidimensional space along which Y of equation (9) is minimised. Each time the algorithm needs an output function value Y for a given multidimensional input vector $\boldsymbol{X}$ (magnet thicknesses), it calls the FE program. The FE program generates a new mesh according to the changed input magnet thicknesses. The program then does the pre-processing and the nonlinear solution to find the magnetic vector potentials. Hence, the torque, flux linkages, supply voltage as well as the new magnet volume are calculated, followed by the calculation of Y according to equation (9). The FE program may be called a number of times by the algorithm during iteration. At the end of each iteration a test is carried out to determine if an absolute minimum has been reached. If not, a next iteration is executed.

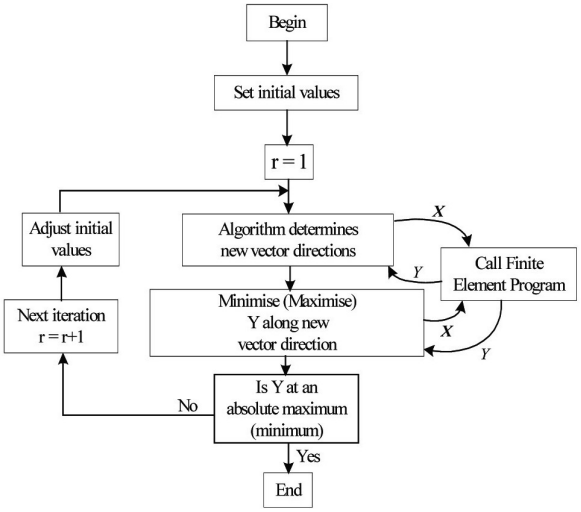

Figure 10: Optimisation procedure using FE solution directly.

5. OPTIMISATION RESULTS

The results of the optimal magnet sheet thicknesses after implementing the optimisation procedure as described in the previous section, are given in Table 1. The type and strength of the PM material used in the design optimisation are also given in Table 1. The PM material used is a new type epoxy-bonded NdFeB magnet material. The flux density of these types of magnets is generally lower than those of sintered magnets. The advantages of the epoxy-bonded magnets are that these magnets are (i) not brittle, (ii) can easily be shaped as required and (iii) are protected against corrosion.

TABLE 1: FINAL OPTIMISED MAGNET THICKNESS

Optimised magnet thickness (mm)		
Inner barrier	Middle barrier	Outer barrier
4.05	2.27	3.07
Material type: bonded rear earth permanent magnet; Hc = 420kA/m; Br = 0.6 Tesla; Density = 6 g/cm^3		

The effect of the PM sheet flux on the q-axis stator flux is shown clearly in Fig. 11. In Fig. 12 a cross-section of the

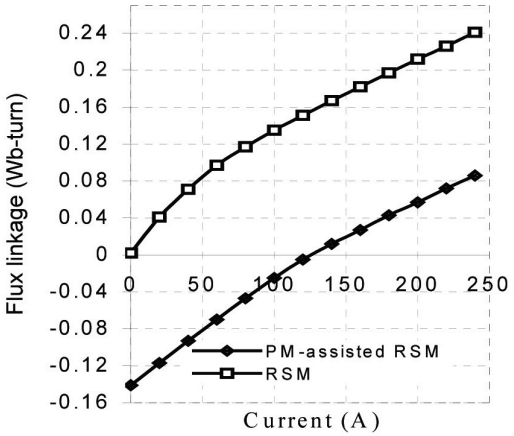

Figure 11: FE calculated *q*-axis flux linkages of the RSM and PM-assisted RSM.

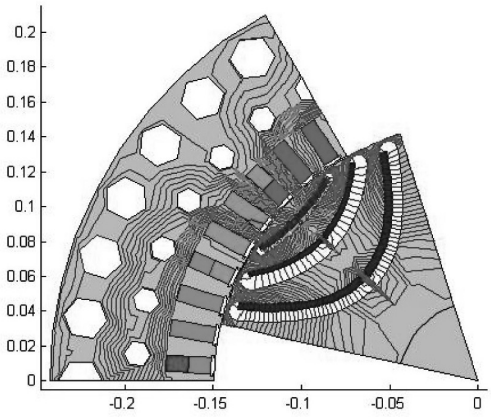

Figure 12: Cross-section of optimal PM-assisted RSM and flux plot with only PMs active.

Figure 13: Cross-section of 110 kW traction RSM with PM sheets incorporated into the reluctance rotor.

optimal PM-assisted RSM together with a field plot with only the magnets active, as an example, are shown. A photo of the actual traction RSM with the PM sheets inside the flux barriers of the reluctance rotor is shown in Fig. 13.

With the addition of the PM sheet material to the reluctance rotor the mechanical strength of the small iron ribs and webs of the rotor must be examined at high speeds. FE mechanical-strength analysis has been conducted on the rotor at an over speed of 3800 r/min. The maximum deflection was found to be 70 μm on the outside of the rotor and the maximum stress of 190 MPa on the inner iron web. These results are well within safety limits.

6. MEASURED RESULTS

A block diagram of the test drive system is shown in Fig. 14. It consists of the power electronic converter (controlled rectifier and inverter), the PM-assisted RSM connected to the dynamometer load, a DSP controller with current and position feedback and DC-bus voltage measurement, and finally the Norma measurement system and star point adapter. The star point adapter is necessary to create a

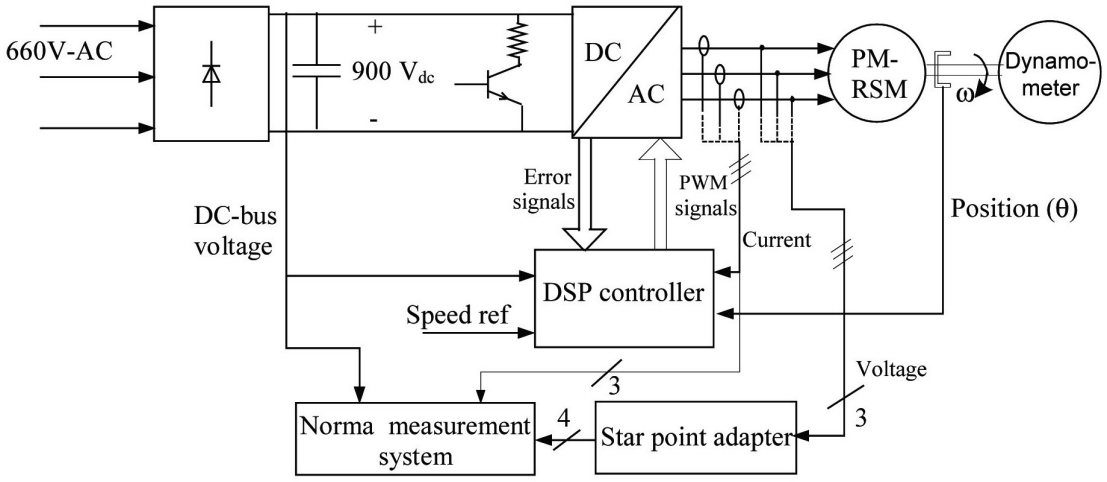

Figure 14: Block diagram of test drive system

neutral (the traction machine has no neutral) for the Norma system for accurate measurement.

In Fig. 15 the measured open circuit phase voltage waveform of the PM-assisted RSM (driven by a DC machine) is shown at the base speed of 1200 r/min. It is clear that the waveform is practically sinusoidal; the high frequency ripple voltage is due to the slotted airgap and unskewed rotor. What is, however, important is the relatively low induced phase voltage of 40 V_{rms} at this speed. This low no-load induced voltage is particularly important, as it implies that the machine can rotate at very high speeds before the induced phase voltage becomes higher than the inverter's rated voltage.

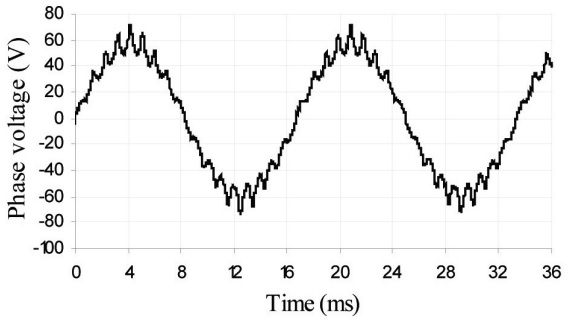

Figure 15: Induced phase voltage of the PM-assisted RSM at 1200 r/min.

Full-load tests were conducted on the RSM and PM-assisted RSM drives at speeds ranging from 800 r/min up to 2800 r/min. The test results were then compared with those of the IM drive. For all the tests the torques of the drives were maximised [by adjusting, amongst other things, the current angle] subject to supply current and voltage constraints; the supply current was limited to 200 A_{rms} and the fundamental supply voltage was limited to 220 V_{rms}/phase.

Figure 16 shows both the FE-calculated and measured torque and voltage characteristics of the RSM, while the FE-calculated and measured torque-speed characteristics of the PM-assisted RSM are compared in Fig. 17. It is evident that good correlation is obtained. The measured

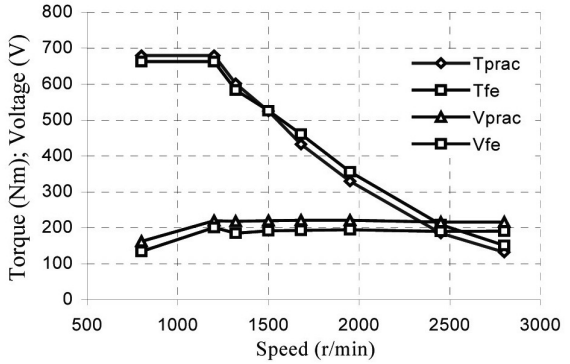

Figure 16: Calculated and measured torque and phase voltage versus speed of RSM.

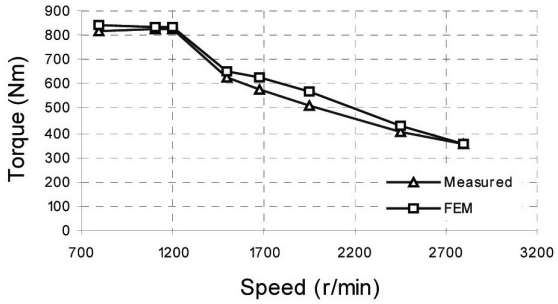

Figure 17: Calculated and measured torque versus speed of PM-assisted RSM (at rated current).

characteristics of the optimum current angle versus speed for the RSM and PM-assisted RSM are shown in Fig. 18. It can be observed that the optimum current angle of the PM-assisted RSM is generally lower than that of the RSM. The current angles for both machines tend to increase sharply as the speed is increased from base speed.

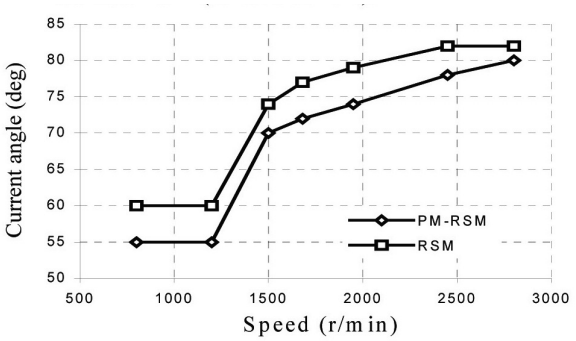

Figure 18: Measured current angle versus speed of the PM-assisted RSM and RSM.

The measured torque results of the PM-assisted RSM, RSM and IM are presented in Fig. 19. It can be seen that the torque of PM-assisted RSM correlates well with that of the IM. The poor torque performance of the RSM in the flux-weakening region is clearly visible. In Fig. 19, PM-RSM1 represents the maximum torque the PM-assisted RSM can produce in the constant torque region and at rated

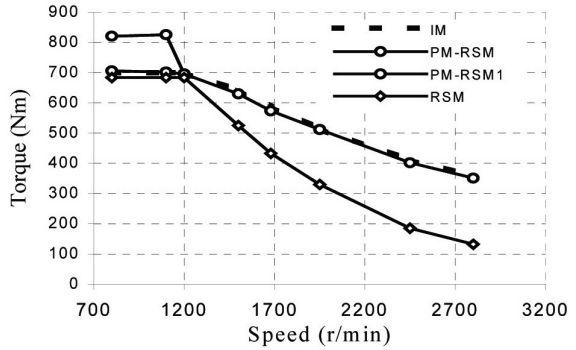

Figure 19: Measured torque versus speed of the IM, PM-assisted RSM and RSM.

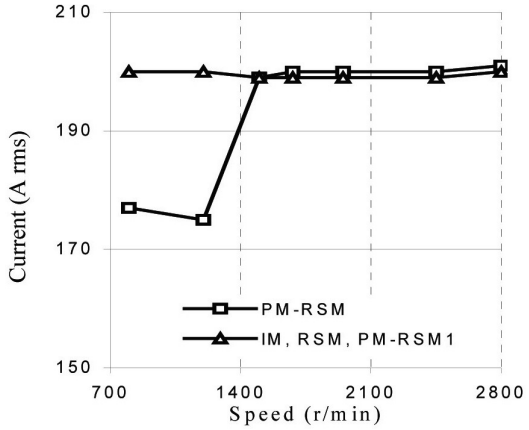

Figure 20: Measured fundamental currents versus speed of the induction machine and pm-assisted rsm.

current subject to voltage constraints. The current versus speed curves of the PM-assisted RSM and IM for the same output power are shown in Fig. 20. It can be seen that for the same output torque the PM-assisted RSM draws less current than that of the IM in the constant torque region. In the flux-weakening region the currents are comparable for both drives.

The measured power factor versus speed curves of the PM-assisted RSM, IM and RSM are shown in Fig. 21. It can be seen that the power factors of the IM and PM-assisted RSM are generally within 2% of each other. The power factor of the pure RSM is always lower compared to the

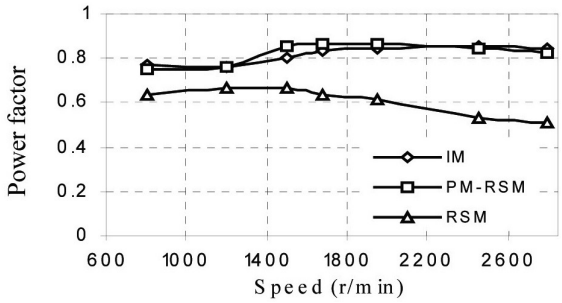

Figure 21: Measured fundamental power factor versus speed of the IM, PM-assisted RSM (PM-RSM) and RSM.

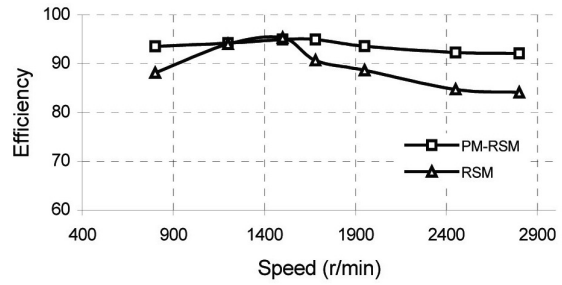

Figure 22: Measured efficiency versus speed of the RSM and PM-assisted RSM.

IM. At maximum speed of 2800 r/min the measured power factor of the RSM is about 0.54 as compared to the power factor of 0.85 of the IM and PM-assisted RSM. Figure 22 shows the efficiency versus speed curves of the RSM and PM-assisted RSM. It is clear that the efficiency of the PM-assisted RSM is significantly higher than that of the RSM.

7. CONCLUSIONS

The following conclusions are reached:

(i) The use of PM-sheets covering the full width of each flux barrier of the reluctance rotor show to induce a very much sinusoidal back EMF voltage in the stator, which is advantageous for the control of the machine.
(ii) The optimum PM-design shows that only a relatively small amount of medium strength bonded PM sheet material is required in an optimum designed RSM rotor to obtain the equivalent flux-weakening torque-speed performance of the conventional IM drive. This has the further advantage of an improved RSM-performance in the constant torque speed region, a higher efficiency and much improved power factor over the whole speed range.
(iii) By minimizing the PM volume used, the cost and the induced back EMF of the machine is reduced. It is shown that, with the required flux-weakening torque-speed performance obtained, the back EMF voltage is only 0.1 per unit at rated speed. This implies low iron losses under open-circuit conditions, which is important for traction applications, e.g. dead hauling of faulty electrical vehicles. It, furthermore, implies that the machine can rotate at substantially high speeds before the induced voltage become higher than the inverter's rated voltage.

REFERENCES

[1] Fratta A. and Vagati F.: "Synchronous reluctance versus induction motor: a comparison", *Proceedings Intelligent Motion (Nűrnberg)*, April 1992, pp. 179-186.

[2] Bomela X.B., Jackson S.K., and Kamper M.J.: "Performance of small and medium power flux barrier rotor reluctance synchronous machine drives", *ICEM* (Istanbul), Sept. 1998, vol. 1, pp. 95-99.

[3] Germishuizen J., Van der Merwe, F.S., Van der Westhuizen, K. and Kamper, M.J.: "Performance comparison of reluctance synchronous and induction traction drives for electrical multiple units", IEEE-IAS Conference (Rome), October 2000.

[4] Sibande S.E.: "Rotor design and performance evaluation of PM-assisted reluctance synchronous traction machine", MSc dissertation, University of Stellenbosch (South Africa), 2005.

[5] Kamper M.J. and Mackay A.T.: "Optimum control of the reluctance synchronous machine with a cageless flux barrier rotor", SAIEE Trans., June 1995, vol. 86, no. 2, pp. 49-56.

[6] Fratta A, Vagati A, Villata F: "Permanent magnet assisted synchronous reluctance drives for constant-power applications", Intelligent Motion Proceedings, 1992.

[7] Lee J.H., Kim J.C., Hyun D.S.: "Effect analysis of magnet on Ld and Lq inductance of permanent magnet assisted synchronous reluctance motor using finite element method", IEEE Trans. MAG-35(3):1199-1202, May 1999.

[8] Morimoto S., Sanada M. and Takeda Y., "Performance of PM-assisted synchronous reluctance motor for high-efficiency and wide constant-power operation", IEEE Trans. IA-37(5): 1234 -1239, 2001.

[9] Haataja J. and Pyrhönen J.: "Permanent magnet assisted synchronous reluctance motor: an alternative motor in variable speed drives", Energy efficiency in motor driven systems, Springer-Verlag, Berlin, (Germany), pp. 101-110, 2003.

[10] Boldea I., Tutelea L., Ilie Pitic C.: "PM-assisted reluctance synchronous motor/generator (PM-RSM) for mild hybrid vehicles: electromagnetic design", IEEE Trans. IA-40(2):492-498, March/April 2004.

[11] Jahns T.M., Kliman G.B. and Neumann T.W.: "Interior PM synchronous motor for adjustable speed drives", IEEE Trans. IA-22(4):738-747, July/August 1986.

[12] Powell M.J.D.: "An efficient method for finding the minimum of a function of several variables without calculating derivatives", Computer Journal, vol. 7, 1964, pp. 155-162.

[13] Kamper M.J, van der Merwe F.S, Williams S.: "Direct finite element design optimisation of cageless reluctance synchronous machine", IEEE Trans. on EC-11(3):547-553, September 1996.